UC San Diego

Title

The Association Between Regional Macula Vessel Density and Central Visual Field Damage in Advanced Glaucoma Eyes

Permalink

https://escholarship.org/uc/item/9h65x5pz

Journal

ISSN

Authors

Ghahari, Elham
Bowd, Christopher
Zangwill, Linda M
et al.

Publication Date

DOI

The association between regional macula vessel density and central visual field damage in advanced glaucoma eyes

Elham Ghahari[1], Christopher Bowd, PhD[1], Linda M. Zangwill, PhD[1], James A. Proudfoot, MSc[1], Rafaella C. Penteado, MD[1], Haksu Kyung[1], Huiyuan Hou, MD, PhD[1], Sasan Moghimi, MD[1], Robert N. Weinreb, MD[1]

[1]Hamilton Glaucoma Center, Shiley Eye Institute, Viterbi Family Department of Ophthalmology, University of California San Diego, La Jolla, CA, United States.

Abstract

Purpose: To evaluate regional and global structure-function relationships between macular vessel density (MVD) assessed by optical coherence tomography angiography (OCTA) and 10–2 visual field (VF) sensitivity in advanced open angle glaucoma eyes.

Methods: Macular OCTA and 10–2 VF sensitivity of 44 patients (MD < −10 dB) were evaluated. Regional and global VF mean sensitivity (MS) was calculated from total deviation plots. Superficial and deep MVD were obtained from 3×3 and 6×6 mm^2 OCTA scans using two sectoral definitions. SDOCT macular ganglion cell complex (GCC) thickness was obtained simultaneously from the same scan as MVD measurements. Linear regression models were used to assess the associations (R^2).

Results: Lower MS was significantly associated with a reduction in superficial MVD and GCC in each region of both scan sizes for both maps. Associations were weaker in the individual sectors of the whole image grid than the ETDRS map. Deep layer MVD was not associated with central MS. Although 6×6 mm^2 and perifoveal vessel density had better associations with central 10° MS compared to GCC thickness (example R^2 from 25.7 to 48.1 μm and 7.8 to 32.5%, respectively), GCC associations were stronger than MVD associations in the central 5° MS.

Conclusions: Given stronger MVD- central 10° VF association compared to GCC, as well as stronger GCC- central 5° VF association compared to MVD, MVD and GCC are complementary measurements in eyes with advanced glaucoma. Longitudinal analysis is needed to determine the relative utility of the GCC and MVD measurements.

Précis:

Both macular superficial vessel density and ganglion cell complex thickness measurement are significantly associated with regional and global 10° central visual field sensitivity in advanced glaucoma.

Keywords

Central visual field; Macula; Advanced Glaucoma; Vessel Density; Thickness

Introduction

Glaucoma affects the optic nerve head, peripapillary retinal nerve fiber layer and corresponding visual field. However, evidence has shown that it also is associated with damage to retinal ganglion cells (RGCs) in the macula that can be confirmed by testing sensitivity of the central 10 degrees of the visual field.[4] As a result, the role of imaging of the inner retinal layers of the macula with spectral-domain optical coherence tomography (SDOCT) in the diagnosis and monitoring of glaucoma has increased. [4, 5–9] We and others recently reported that among SDOCT structural measurements, thickness of the macular ganglion cell inner plexiform layer (GCIPL) is a promising measurement for detecting progression in advanced glaucoma eyes compared to papillary or parapapillary thickness measurements because this measurement presents a lower measurement floor (a structural thickness measurement after which no measurable decrease in thickness can be measured) than other measurements investigated. [5–6, 10–11]

Although the pathogenesis of primary open angle glaucoma (POAG) is not fully understood, there is consistent evidence that vascular factors are involved.[1, 12, 13] The development of optical coherence tomography angiography (OCTA) has allowed non-invasive evaluation of the perfused microvasculature of the optic nerve, peripapillary retina, and macula at various depths.[14–19]

Reduced circumpapillary vascular density (cpMVD) has been reported in glaucomatous eyes. [16, 20] Significant regional associations between cpMVD and corresponding 24–2 mean sensitivity values in moderate-to-advanced glaucoma also have been observed.[21] We recently reported that macula vessel density dropout was detectable in preperimetric and early POAG eyes.[22]

Global associations between whole macula and parafoveal vessel densities and visual field 24–2 mean deviation (MD) in advanced disease have been reported.[23] However, it is not currently clear whether there are significant regional associations between macular vessel densities and corresponding visual field 10–2 test points in advanced glaucoma eyes. The primary purpose of the current study was to investigate regional macular vessel density-visual sensitivity associations using OCTA and 10–2 test pattern standard automated perimetry visual field (VF) testing within both 3×3 and 6×6 mm^2 regions using the whole image grid and the ETDRS map. We also sought to compare the strength of these

associations with local SDOCT-measured ganglion cell complex (GCC) thickness-visual sensitivity associations.

Methods

The current study is a cross-sectional study including patients with advanced primary open-angle glaucoma from the Diagnostic Innovations in Glaucoma Study (DIGS). The DIGS is an ongoing prospective, longitudinal study at the Hamilton Glaucoma Center, University of California, San Diego, designed to evaluate ocular structure and visual function in glaucoma. Details of the DIGS protocol have been described previously.[24] All methods adhered to the tenets of the Declaration of Helsinki and the Health Insurance Portability and Accountability Act and were approved by the institutional review boards at the University of California, San Diego. Informed consent was obtained from all participants.

One eye with advanced glaucoma (Humphrey visual field MD < −10 dB) from each of 44 primary open-angle glaucoma patients aged >18 years with best-corrected visual acuity (BCVA) 20/40 was included. Eyes with a history of ocular intervention other than uncomplicated cataract or uncomplicated glaucoma surgery or with intraocular disease (e.g., diabetic retinopathy or non- glaucomatous optic neuropathy) were excluded as were individuals with systemic disease that could have an impact on study results (e.g., stroke or pituitary tumor). Individuals with systemic hypertension and diabetes mellitus without diabetic or hypertensive retinopathy were not excluded.

Eyes classified as POAG had glaucomatous optic nerve damage (focal narrowing or notching of the neuroretinal rim or localized or diffuse atrophy of the retinal nerve fiber layer by masked stereoscopic optic disc photograph assessment) with associated Humphrey 24–2 SITA VF results outside of normal limits (ONL). ONL tests had a Glaucoma Hemifield Test (GHT) result outside of normal limits or a pattern standard deviation (PSD) outside 95% normal limits confirmed on 2 consecutive, reliable tests. Reliable tests required fixation losses 33% and false positives 33% with no evidence of rim or eyelid artifacts, inattention or fatigue as assessed by instrument operators or UCSD Visual Field Assessment Center personnel.

For the present analyses, central VF testing was performed using the 10–2 SITA protocol. In order to avoid learning effects, all participants who were included were familiar with VF testing from earlier exposure to at least 2 VF examinations. All visual field 10–2 total deviation map testing points' threshold sensitivities in dB were unlogged to 1/Lambert values. VF sensitivity was calculated by averaging threshold sensitivity values (1/Lambert) from all test points within the visual field sectors corresponding to the anatomic sectors described below. Averaged unlogged threshold sensitivity values used for statistical analysis.

All study participants underwent ophthalmological examination, including assessment of BCVA, slit- lamp biomicroscopy, intraocular pressure (IOP) measurement with Goldmann applanation tonometry, gonioscopy, central corneal thickness (CCT) measured with ultrasound pachymetry (DGH Technology Inc., Exton, PA), dilated fundus examination, simultaneous stereo photography of the optic disc, and standard automated perimetry.

Systemic measurements included systolic and diastolic blood pressure and pulse rate measured with an Omron Automatic blood pressure instrument (model BP791IT; Omron Healthcare, Inc., Lake Forest, IL). Mean arterial pressure was calculated as 1/3 systolic blood pressure + 2/3 diastolic blood pressure. Mean ocular perfusion pressure was defined as the difference between 2/3 of mean arterial pressure and IOP.

Optical coherence tomography angiography and spectral domain OCT

OCTA and SDOCT imaging of the macula were performed with the Avanti spectral-domain OCT (software version 2017, 1, 0,144; Optovue, Inc., Fremont, CA). Avanti imaging and VF testing were completed within one year (median 30 days, with range of 0–365 and inner quartile range (Q1-Q3) of 1 – 125 days). The OCT Angiovue system incorporated in the Avanti SDOCT system uses a split-spectrum amplitude-decorrelation angiography (SSADA) method to capture the dynamic motion of the red blood cells and provide a high-resolution 3-dimensional visualization of the vascular structures at various user-defined layers of the retina at the capillary level. Vessel density is automatically calculated as the percentage of a measured area occupied by flowing blood vessels defined as pixels having decorrelation values above the threshold level directly derived from SDOCT B-scans. The SDOCT image consists of a series of B-scans with 2 rapid repeats at each B-scan location, and the average of the 2 repeated B-scans forms the conventional SDOCT intensity image. The amplitude decorrelation between these 2 B-scans forms the OCTA image. Because the OCTA image and SDOCT intensity image are based on the same B-scans, there is pixel-to-pixel co-localization between the OCTA image volume and the SDOCT intensity image and no need for alignment.

Superficial macular vessel density measurements were calculated from both 3×3 mm^2 and 6×6 mm^2 scans centered on the fovea composed of merged Fast-X (horizontal) and Fast-Y (vertical) volume scans of 304 B-scans X 304 A-scans per B-scan in a slab from 3 μm below the internal limiting membrane (ILM) to 10μm below the inner plexiform layer (IPL). Deep macular vessel density measurement was calculated from 10μm below the IPL to 10μm above the outer plexiform layer. Parafoveal vessel density measurements were calculated within an instrument defined annulus with an inner diameter of 1 mm and outer diameter of 3 mm for both 3×3 mm^2 and 6×6 mm^2 macular scans. Perifoveal vessel density measurements were calculated within an instrument defined annulus with an inner diameter of 3 mm and outer diameter of 6 mm for 6×6 mm^2 macular scans centered on the fovea, using two sectoral definitions 1) whole image grid and 2) ETDRS pattern (Figure 1). ETDRS stands for Early Treatment Diabetic Retinopathy Study (ETDRS) map. We used a pre-defined, modified ETDRS map in this study and name it as ETDRS map through the paper for the sake of simplicity.

Macular ganglion cell complex (GCC) thicknesses were obtained from the same 3×3 mm^2 and 6×6 mm^2 scans as macular vessel densities centered on the fovea from the ILM to the IPL consisting of the ganglion cell layer, IPL, and RNFL.

Trained graders reviewed the quality of all Avanti OCTA and SDOCT scans using a standard protocol established by the Imaging Data Evaluation and Analysis (IDEA) reading center at University of California, San Diego. Poor-quality scans were excluded from the analysis if

signal strength index was <4; (2) image clarity was poor; (3) local signal was weak due to artifacts such as floaters; (4) residual motion artifacts were visible on the enface angiogram; and (5) segmentation failures were evident.

Mapping Structure (vessel density and GCC thickness) to Function (VF mean sensitivity)

VF 10–2 total deviation map threshold sensitivity (dB) was used for functional measurements. RGC displacement at the macula was adjusted by using equations derived from the histological analysis to approximate the location of the RGCs with each SAP test point.[25] Because one degree of a visual angle equals 0.3 mm on the retina, [26] the correspondence map for structure-function evaluation at the macula was defined by VF points corresponding to the OCTA 3×3 mm^2 and 6×6 mm^2 scan size whole image grid and ETDRS maps parameters. (Figure 2)

Statistical analysis

Clinical characteristics, OCTA-derived vessel densities, and OCT-derived tissue thicknesses were described as mean values with associated 95% confidence intervals. Linear mixed effects models were used to investigate univariable associations between VF total deviation threshold sensitivity and vessel density and tissue thickness measurements, with multivariable models fit including age and scan quality indices as covariates. Confidence intervals for adjusted R^2 in the multivariable analysis were derived from 5000 bootstrap resamples. To compare the strength of their association with VF parameters, vessel density and thickness parameters corresponding to the same VF region were included as covariates in multivariable linear regression models along with age and scan quality. All statistical analyses were performed with R version 3.5.2. The alpha level (type I error) was set at 0.05.

Results

Forty-four eyes of 44 advanced glaucoma patients were included in this cross-sectional study. Demographics and clinical characteristics of the study population are summarized in Table 1. Mean (Range) of OCTA vessel density and thickness parameters defined by whole image grid and ETDRS maps for 3×3 and 6×6 mm^2 scans are shown in Supplemental Tables 2 and 3, respectively. The results of univariable and multivariable (adjusted for age and scan quality) linear regression analyses between regional and global macular vascular and structural parameters and 10–2 mean sensitivities (expressed in decibel scales) for 3×3 mm^2 and 6×6 mm^2 scans are shown in Supplemental Tables 4 and 5, respectively and Figure 3 and 4. Superficial macular vessel density and GCC thickness decreased with worsening central VF mean sensitivity in each region of the 3×3 and 6×6 mm^2 scans with parafovea ETDRS map R^2 values of 37.7 (p<0.001) and 43.1 (p<0.001) for 3×3 mm^2 scan and 20.9 (p=0.001) and 17.8 (p=0.003) for 6×6 mm^2 scan, respectively. Each 1 dB decrease in central VF mean sensitivity was associated with a reduction of 0.45% and 1.26 μm for 3×3 mm^2 and 0.28% and 0.68 μm for 6×6 mm^2 parafovea ETDRS map vessel density and GCC thickness, respectively. Associations were generally weaker in the individual sectors of the whole image grid (R^2 ranging from ~0% to 22.2% in univariable analysis and 1.6% to 37.2% in multivariable analysis) than the ETDRS sectors (R^2 ranging from 16.9% to 29.4% in univariable analysis and 30.9% to 48.1% in multivariable analysis).

In 3×3 mm^2 scans, in general, stronger global and regional associations (larger R^2) were found between central VF sensitivity and GCC thickness than vessel density, but the differences did not reach statistical significance. As an example, R^2 ranges from 36.3 to 56.7 μm for GCC and 30.1 to 37.7% for vessel density of 3×3 mm^2 scan (p >0.05).

Model parameters for both were similar when age and image quality were included as covariates in multivariable analysis in the 6×6 mm^2 inner circle of the ETDRS map (Figure 3). GCC/VF sensitivity associations were slightly weaker compared to vessel density/VF sensitivity associations in the outer ring (3–6 mm) and whole ETDRS (1–6 mm) of the 6×6 mm^2 scan in the inferior hemisphere, where we observed worse VF mean sensitivity.

Although superficial macular vessel density and GCC thickness measurements were both significantly associated with mean sensitivity in central 5° VF (i.e. 3×3 mm^2 scans and inner circle of the 6×6 mm^2 scans) using both ETDRS and whole image grid maps, univariable analysis showed GCC/VF sensitivity associations were stronger (e.g.: 3×3 scan: R^2 ranged from 36.3% (whole image of whole image grid) to 56.7% (parafovea superior hemifield ETDRS map) than vessel density/VF sensitivity associations (e.g.: 3×3 scan: R^2 ranged from 30.1% (whole image of whole image grid) to 37.7% (parafoveal ETDRS map), Supplemental Tables 4, 5 and Table 6). The magnitude of microvascular dropout and thinning to reach 1 dB in central 5° VF of 3×3 mm^2 scans ranged between 0.32% to 0.47% for superficial vessel density and 0.91% to 1.48% for GCC thickness when age and image quality were included as covariates in multivariable analysis.

A summary of the multivariable linear regressions for VF mean sensitivity with both vessel density and GCC thickness parameters, as well as age and scan quality, is available in Table 6. GCC thickness had a stronger association with VF mean sensitivity compared to vessel density in both the ETDRS and whole image grid maps of the 3×3 mm^2 scans. Both vessel density and GCC thickness were significantly associated with VF mean sensitivity in the inferior hemisphere and whole ETDRS of the inner circle (1–3 mm) of the 6×6 mm^2 scan. Vessel density had a stronger association with VF mean sensitivity compared to GCC thickness in the inferior and whole hemispheres in the outer ring (3–6 mm), whole ETDRS (1–6 mm), and whole image of the 6×6 mm^2 whole image grid map, where at this map locations we observed worse VF mean sensitivity.

Deep layer macular vessel density was not associated with central visual mean sensitivity (Supplemental Table 4 and 5, and Figure 4).

Discussion

In the current study, SDOCT superficial MVD (measured using OCTA) and GCC thickness were significantly associated with regional and global central 10–2 test pattern visual field sensitivity in advanced primary open-angle glaucoma eyes. Superficial MVD and GCC thickness measurements both decreased with decreasing mean sensitivity in the central 10°. 6×6 mm^2 and perifoveal vessel density had better associations with central 10° VF mean sensitivity compared to GCC thickness in advanced glaucoma. However, GCC thickness

measurements were more strongly correlated with central 5° mean sensitivity compared to superficial macular vessel density in these eyes.

We found no associations between deep layer vascular measurements of the macula and central VF sensitivity despite investigating associations using different scan patterns and image sizes. Superficial macular vessel density is responsible for blood supply to nerve fiber, ganglion cell, and inner plexiform layers, which are the primary sites of glaucomatous damage. [27, 28] The current results are consistent with the results of previous studies reporting that glaucoma affects the superficial macular vessel density more than the deep layer vessel density.[29–31]

In glaucomatous eyes, Takusagawa et al, [29] found a greater diagnostic accuracy and vessel density loss over the global 6×6 mm^2 region compared to studies that reported over a 3×3 mm^2 region. Rao et al [32] compared the diagnostic accuracy of vessel density reduction over both a 3×3 and 6×6 mm^2 macular scan sizes and reported that the outer circle measurements of the 6×6 mm^2 macular scans seem to be better than the inner circle measurements in diagnosing glaucoma. In their study, inner circle vessel density measurements, equal to 3×3 mm^2 scan size, were statistically similar to the control eyes. They concluded that the evaluation of superficial macular vessel density in the central 3×3 mm^2 region, especially on a 6×6 mm^2 OCTA scan, has little value for diagnosing POAG. In a recent study by our team [33], we evaluated the diagnostic accuracy of 3×3 and 6×6 mm^2 macula OCTA scans for differentiating healthy, mild glaucoma, and moderate to severe glaucoma eyes. The outer area of the 6×6 mm^2 scan size vessel density had higher diagnostic accuracy compared with the inner area of the 3×3 mm^2 scan when differentiating between healthy and mild glaucoma and similar diagnostic accuracy when differentiating between healthy and moderate to severe glaucoma eyes.

Our current results are indirectly consistent with previously mentioned studies. We found generally stronger associations between central 10° visual field sensitivity and MVD compared to GCC thickness. The exception is that 3X3 mm^2 GCC thickness had better associations with central 5° visual field sensitivity compared to MVD. This may be related to the possibility that the GCC thickness has already thinned in the perifovea before MVD attenuation. Additional longitudinal studies are required to investigate the temporal relationship between regional GCC thickness and vessel density loss at the advanced stages of the glaucoma disease. We found that vessel density/VF mean sensitivity association is significant over a relatively larger area i.e., across whole 6×6 mm^2 scan size compared to GCC thickness/VF mean sensitivity association. GCC thickness was more strongly associated with severity of visual field loss within 5° (3×3 mm^2 scan size and inner circle of 6×6 mm^2 scan size) compared to 5° to 10° (outer circle of 6×6 mm^2 scan size) and whole 10° of the central visual field. Our study result regarding GCC thickness/VF mean sensitivity association is consistent with other reports [34–45] which suggests that macular thickness measurements are more associated with the severity of central degrees of visual field loss compared to vessel density.

In this study, MVD showed a significant relationship in the entire 10° of the central visual field. Considering the range of VF sensitivity at which thickness measurement floor begins,

[36]–[38] and large fluctuations of VF tests in patients with advanced glaucoma, [38]–[40] detecting actual glaucomatous change and disease progression is challenging. Our finding that the MVD/VF sensitivity association is stronger over a relatively larger area of central VF compared to the association between GCC thickness and VF sensitivity suggests that MVD may be a useful parameter for monitoring advanced glaucoma. This is particularly relevant as MVD does not have a detectable measurement floor. [41]

We investigated regional macular structure-function association in addition to global macular structure-function association to obtain insight for improving structure- function mapping. Thus, in regions with stronger association, early changes in macular OCTA vessel densities, with a lower detectable measurement floor, might assist clinicians to detect changes in advanced glaucoma eyes so that they can determine when to intensify treatment, either medically or surgically.

Another big advantage is that structural/vascular assessment is not dependent on patient response and may thus yield less variable results compared to visual field testing. However, given the worse reproducibility of vessel density measurements, and the large proportion of eyes with poor quality OCTA scans the utility of including OCTA for monitoring advanced glaucoma eyes may be limited.

The strength of the current study is including macular vessel density and GCC thickness measurements over the same scan size, which provided a direct comparison of association with central visual field sensitivity between the two measurements in advanced glaucoma eyes. There are several limitations to the present study. This study was cross-sectional, so we could not determine if structural damage precede functional damage or vice versa. Reduced retinal microvasculature in advanced glaucomatous eyes could be a result of glaucoma pathophysiology related to tissue thinning or it could be an independent cause of decreased visual sensitivity. Longitudinal studies are necessary to clarify these relationships by determining the temporal course of changes. We did not evaluate the potentially confounding impact of anti-glaucoma drops, BP-lowering medications, and systemic conditions on the vascular measurements. Therefore, we cannot dismiss the effect of these factors on vascular measurements. The effect of ocular and systemic conditions and the use of medications on vascular measurements is an important and topic worthy of further studies. The result presented here might not necessarily generalizable to other instruments' OCTA vessel density or SDOCT macular thickness measurements. Some sectors of the whole image grid don't follow the nature of glaucomatous damage by involving areas from both hemifields, and incorporating very few VF locations. To date, the data on the correlation of vessel density loss and nature of glaucomatous damage is not solid. Hence, we incorporated two different maps. Moreover, void of controls or comparison group limits applicability to nonadvanced open-angle glaucomatous eyes. Given variability of OCTA measurements, observed differences in R^2 values in our study might be affected by limitations of the model fitting procedures. For example, we assume homogenous error variance across the range of OCTA parameter values. Our sample size limits our ability to formally test this assumption. Finally, it is possible that the associations between structural and functional measurements varied in strength across the observed range of MD within the current cohort. To address this, we examined both linear and nonlinear (quadratic) models

as well as locally smoothed fit (LOESS) and its confidence bounds. Our result showed that both the linear and quadratic fit were within LOESS bounds. Therefore, we concluded linear fit is a decent representation of the data and report it in the manuscript.

In conclusion, we found that perifoveal and global superficial MVD measurements were more significantly correlated with central 10° VF mean sensitivity compared to GCC thickness in patients with advanced glaucoma eyes. However, GCC thickness was more strongly correlated with severity of central VF loss within the central 5° compared to vessel density. Longitudinal studies are needed to determine whether these cross-sectional trends in the strength of the associations of perifoveal and parafoveal macula vessel density and GCC thickness with central visual field damage can be used to improve the monitoring of advanced glaucoma.

Supplementary Material

Refer to Web version on PubMed Central for supplementary material.

Acknowledgments
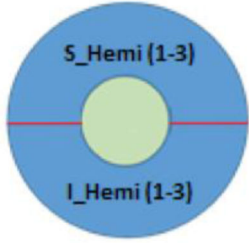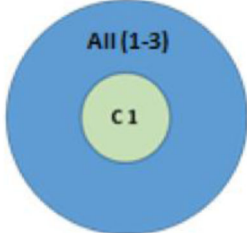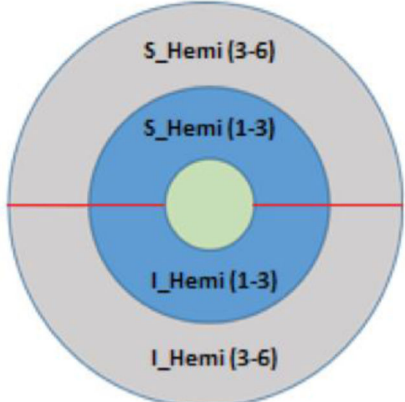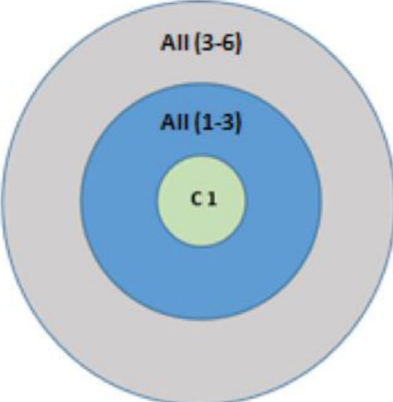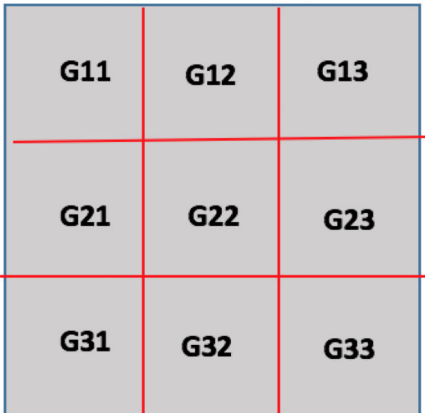
REFERENCES

1-. Weinreb RN, Khaw PT. Primary open-angle glaucoma. Lancet. 2004;363:1711–1720. [PubMed: 15158634]

2. Quigley HA Broman AT. The number of people with glaucoma worldwide in 2010 and 2020. Br J Ophthalmol. 2006;90:262–267. [PubMed: 16488940]

3. Traverso C, Walt J, Kelly S, et al. Direct costs of glaucoma and severity of the disease: a multinational long-term study of resource utilization in Europe. Br J Ophthalmol. 2005;89:1245–1249. [PubMed: 16170109]

4-. Hood DC. Improving our understanding, and detection, of glaucomatous damage: An approach based upon optical coherence tomography (OCT). Prog Retin Eye Res. 2017;57:46–75. [PubMed: 28012881]

5-. Bowd C, Zangwill LM, Weinreb RN, et al. Estimating Optical Coherence Tomography Structural Measurement Floors to Improve Detection of Progression in Advanced Glaucoma. Am J Ophthalmol. 2017;175:37–44. [PubMed: 27914978]

6-. Belghith A, Medeiros FA, Bowd C, et al. Structural Change Can Be Detected in Advanced-Glaucoma Eyes. Invest Ophthalmol Vis Sci. 2016;57:511–518.

7-. Mwanza JC, Durbin MK, Budenz DL, et al. Glaucoma diagnostic accuracy of ganglion cell-inner plexiform layer thickness: comparison with nerve fiber layer and optic nerve head. Ophthalmology. 2012;119:1151–1158. [PubMed: 22365056]

8-. Rao HL, Zangwill LM, Weinreb RN, et al. Comparison of different spectral domain optical coherence tomography scanning areas for glaucoma diagnosis. Ophthalmology. 2010;117:1692–1699. [PubMed: 20493529]

9-. Miraftabi A, Amini N, Morales E, et al. Macular SD-OCT outcome measures: comparison of local structure-function relationships and dynamic range. Invest Ophthalmol Vis Sci. 2016;57:4815–4823. [PubMed: 27623336]

10-. Sung KR, Sun JH, Na JH, et al. Progression detection capability of macular thickness in advanced glaucomatous eyes. Ophthalmology. 2012;119:308–313. [PubMed: 22182800]

11-. Shin JW, Sung KR, Lee GC, et al. Ganglion cell–inner plexiform layer change detected by optical coherence tomography indicates progression in advanced glaucoma. Ophthalmology. 2017;124:1466–1474. [PubMed: 28549518]

12-. Leske MC, Wu SY, Hennis A, et al. Risk factors for incident open-angle glaucoma: the Barbados Eye Studies. Ophthalmology. 2008;85–93. [PubMed: 17629563]

13-. Leske MC, Heijl A, Hyman L, et al. Predictors of long-term progression in the Early Manifest Glaucoma Trial. Ophthalmology. 2007;1965–1972. [PubMed: 17628686]

14-. Jia Y, Wei E, Wang X, et al. Optical coherence tomography angiography of optic disc perfusion in glaucoma. Ophthalmology. 2014;121:1322–3132. [PubMed: 24629312]

15-. Yu J, Jiang C, Wang X, et al. Macular perfusion in healthy Chinese: an optical coherence tomography angiogram study. Invest Ophthalmol Vis Sci. 2015;56:3212–3217. [PubMed: 26024105]

16-. Liu L, Jia Y, Takusagawa HL, et al. Optical coherence tomography angiography of the peripapillary retina in glaucoma. JAMA Ophthalmol. 2015;133:1045–1052. [PubMed: 26203793]

17-. Zhang M, Hwang TS, Dongye C, et al. Automated Quantification of Nonperfusion in Three Retinal Plexuses Using Projection-Resolved Optical Coherence Tomography Angiography in Diabetic Retinopathy. Invest Ophthalmol Vis Sci. 2016;57:5101–5106. [PubMed: 27699408]

18-. Shahlaee A, Samara WA, Hsu J, et al. In Vivo Assessment of Macular Vascular Density in Healthy Human Eyes Using Optical Coherence Tomography Angiography. Am J Ophthalmol. 2016;165:39–46. [PubMed: 26921803]

19-. Spaide RF, Klancnik JM Jr, Cooney MJ. Retinal vascular layers imaged by fluorescein angiography and optical coherence tomography angiography. JAMA Ophthalmol. 2015;133:45–50. [PubMed: 25317632]

20-. Bojikian KD, Chen CL, Wen JC, et al. Optic disc perfusion in primary open angle and normal tension Glaucoma eyes using optical coherence tomography-based microangiography. PLoS One. 2016;11:e0154691.

21-. Shin JW, Lee J, Kwon J, et al. Regional vascular density–visual field sensitivity relationship in glaucoma according to disease severity. Br J Ophthalmol. 2017;101:1666–1672. [PubMed: 28432111]

22-. Hou H, Moghimi S, Zangwill LM, et al. Macula Vessel Density and Thickness in Early Primary Open-Angle Glaucoma. Am J Ophthalmol. 2019;199:120–132. [PubMed: 30496723]

23-. Ghahari E, Bowd C, Zangwill LM, et al. Association of Macular and Circumpapillary Microvasculature with Visual Field Sensitivity in Advanced Glaucoma. Am J Ophthalmol. 2019 Mar 13. [Epub ahead of print].

24-. Sample PA, Girkin CA, Zangwill LM, et al. The African Descent and Glaucoma Evaluation Study (ADAGES): design and baseline data. Arch Ophthalmol. 2009;127:1136–1145. [PubMed: 19752422]

25-. Hood DC, Raza AS. Method for comparing visual field defects to local RNFL and RGC damage seen on frequency domain OCT in patients with glaucoma. Biomed Opt Express. 2011;2:1097–1105. [PubMed: 21559122]

26-. Drasdo N, Millican CL, Katholi CR, Curcio CA. The length of Henle fibers in the human retina and a model of ganglion receptive field density in the visual field. Vision Res. 2007;47(22):2901–11. [PubMed: 17320143]

27-. Provis JM. Development of the primate retinal vasculature. Progress in retinal and eye research. 2001;20:799–821. [PubMed: 11587918]

28-. Snodderly DM, Weinhaus RS, Choi JC. Neural-vascular relationships in central retina of macaque monkeys (Macaca fascicularis). J Neurosci. 1992;12(4):1169–1193. [PubMed: 1556592]

29-. Takusagawa HL, Liu L, Ma KN, et al. Projection-Resolved Optical Coherence Tomography Angiography of Macular Retinal Circulation in Glaucoma. Ophthalmology. 2017;124:1589–1599. [PubMed: 28676279]

30-. Campbell JP, Zhang M, Hwang TS, et al. Detailed Vascular Anatomy of the Human Retina by Projection-Resolved Optical Coherence Tomography Angiography. Sci Rep. 2017;10;7:42201. [PubMed: 28127059]

31-. Chen HS, Liu CH, Wu WC, et al. Optical coherence tomography angiography of the superficial microvasculature in the macular and peripapillary areas in glaucomatous and healthy eyes. Invest Ophthalmol Vis Sci. 2017;58,3637–3645. [PubMed: 28728171]

32-. Rao HL, Riyazuddin M, Dasari S, et al. Diagnostic Abilities of the Optical Microangiography Parameters of the 3×3 mm and 6×6 mm Macular Scans in Glaucoma. J Glaucoma. 2018;27:496–503. [PubMed: 29578891]

33-. Penteado RC, Bowd C, Proudfoot JA, et al. Diagnostic Ability of Optical Coherence Tomography Angiography Macula Vessel Density for the Diagnosis of Glaucoma Using Difference Scan Sizes. J Glaucoma. 2020;29:245–251. [PubMed: 31977545]

34-. Ohkubo S, Higashide T, Udagawa S, et al. Focal relationship between structure and function within the central 10 degrees in glaucoma. Invest Ophthalmol Vis Sci. 2014;55:5269–5277. [PubMed: 25082882]

35-. Raza AS, Cho J, de Moraes CG, et al. Retinal ganglion cell layer thickness and local visual field sensitivity in glaucoma. Arch Ophthalmol. 2011;129:1529–1536. [PubMed: 22159673]

36-. Mwanza JC, Kim HY, Budenz DL, et al. Residual and dynamic range of retinal nerve fiber layer thickness in glaucoma: comparison of three OCT platforms. Invest Ophthalmol Vis Sci. 2015;56:6344–6351. [PubMed: 26436887]

37-. Banister K, Boachie C, Bourne R, et al. Can automated imaging for optic disc and retinal nerve fiber layer analysis aid glaucoma detection? Ophthalmology. 2016;123:930–938. [PubMed: 27016459]

38-. Mwanza JC, Budenz DL, Warren JL, et al. Retinal nerve fibre layer thickness floor and corresponding functional loss in glaucoma. Br J Ophthalmol. 2015;99:732–737. [PubMed: 25492547]

39. Hood DC, Kardon RH. A framework for comparing structural and functional measures of glaucomatous damage. Prog Retin Eye Res. 2007;26:688–710. [PubMed: 17889587]

40-. Gardiner SK, Swanson WH, Goren D, et al. Assessment of the reliability of standard automated perimetry in regions of glaucomatous damage. Ophthalmology. 2014;121:1359–1369. [PubMed: 24629617]

41-. Moghimi S, Bowd C, Zangwill LM, et al. Measurement Floors and Dynamic Ranges of OCT and OCT Angiography in Glaucoma. Ophthalmology. 2019;126:980–988. [PubMed: 30858023]

ETDRS Map	Hemisphere	Full ring
3x3 mm² scan OD	S_Hemi (1-3) / I_Hemi (1-3)	All (1-3) / C 1
6x6 mm² scan OD	S_Hemi (3-6) / S_Hemi (1-3) / I_Hemi (1-3) / I_Hemi (3-6)	All (3-6) / All (1-3) / C 1
Whole Image Grid Map	Whole Image Grid 3x3 mm² scan OD	Whole Image Grid 6x6 mm² scan OD
	G11 G12 G13 / G21 G22 G23 / G31 G32 G33	G11 G12 G13 / G21 G22 G23 / G31 G32 G33

Figure 1.

Schematic macular vessel density map. 3×3 mm² scan: S_Hemi (1–3), I_Hemi (1–3), All (1–3): superior parafovea, inferior parafovea, whole parafovea, respectively. 6×6 mm² scan: S_Hemi (1–6), I_Hemi (1–6), All (1–6): superior hemifield, inferior hemifield, whole field, respectively which are average of 1–3 and 3–6 in each area.
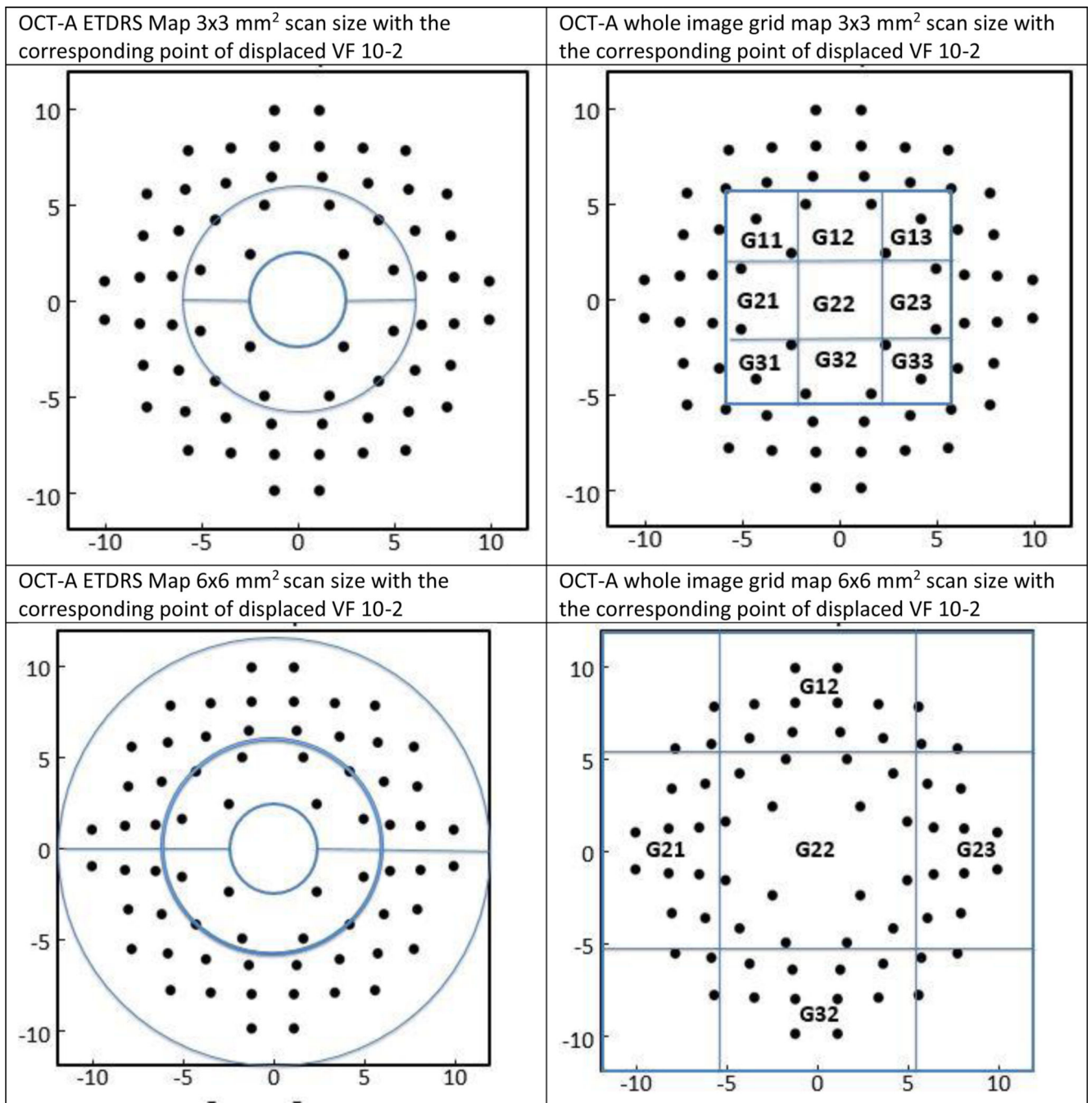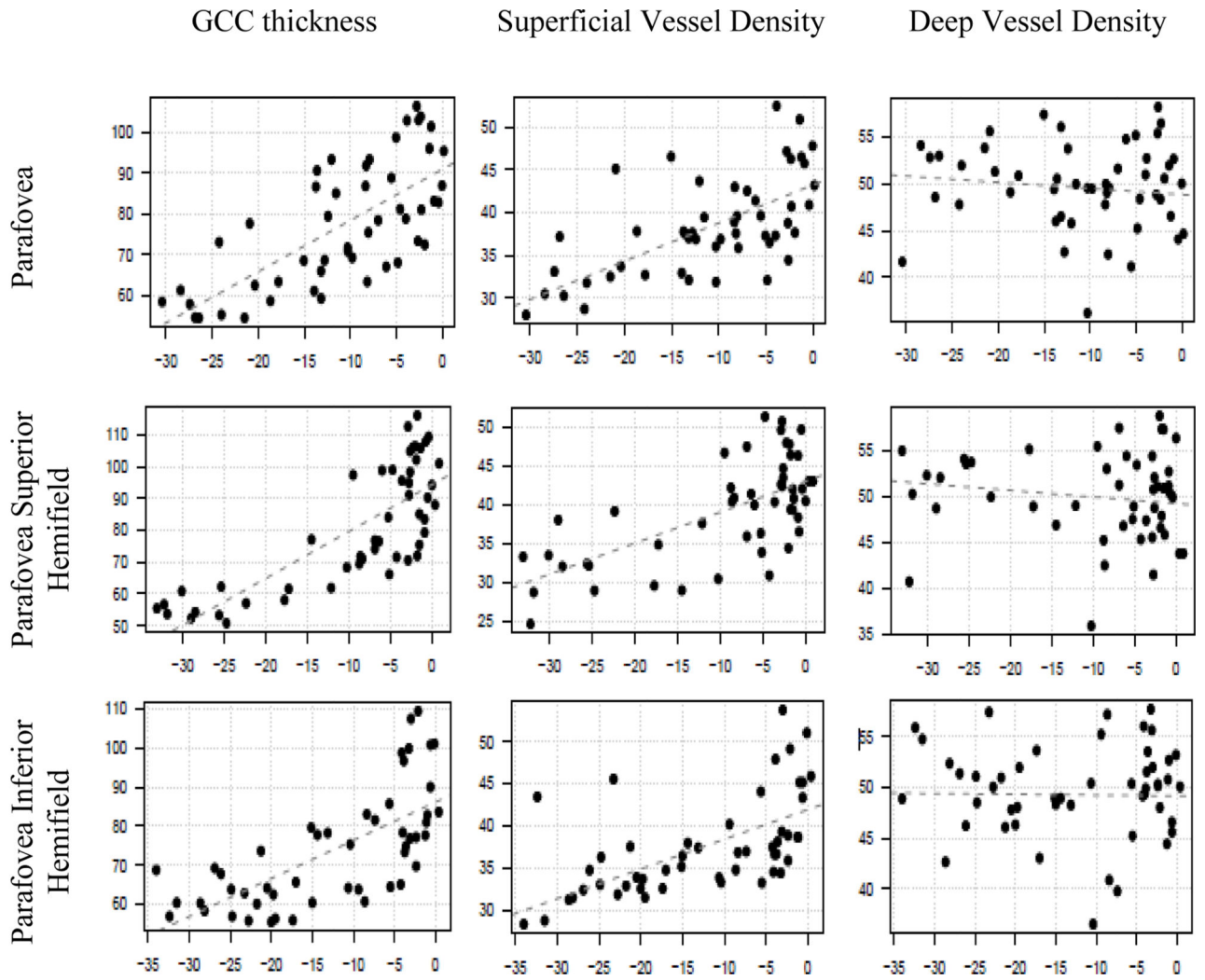
Figure 2.
Schematic map of right eye macular structure-function relationship in advanced glaucoma eyes using a visual field 10–2 adjusted for retinal ganglion cell displacement, and optical coherence tomography angiography (OCT-A) vascular map. The area covered by the 10–2 visual field (black dots) compared with the area covered by the 3×3 mm^2 and 6×6 mm^2 OCT-A scan (blue square and circle).
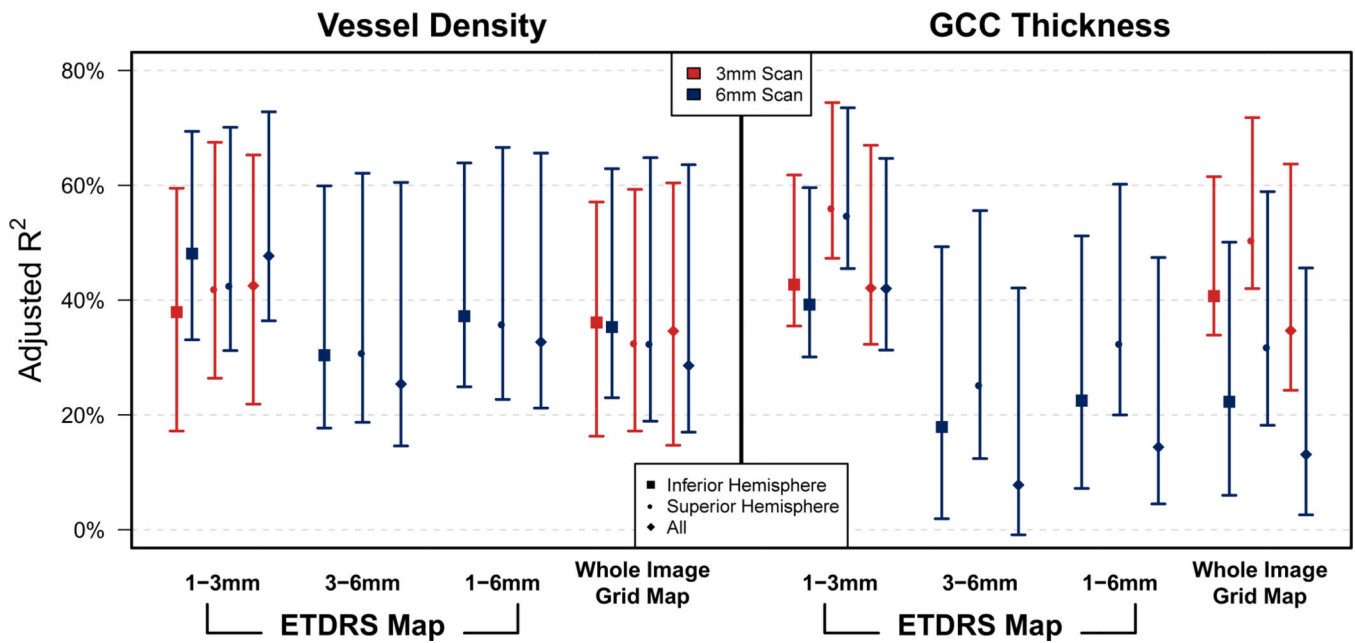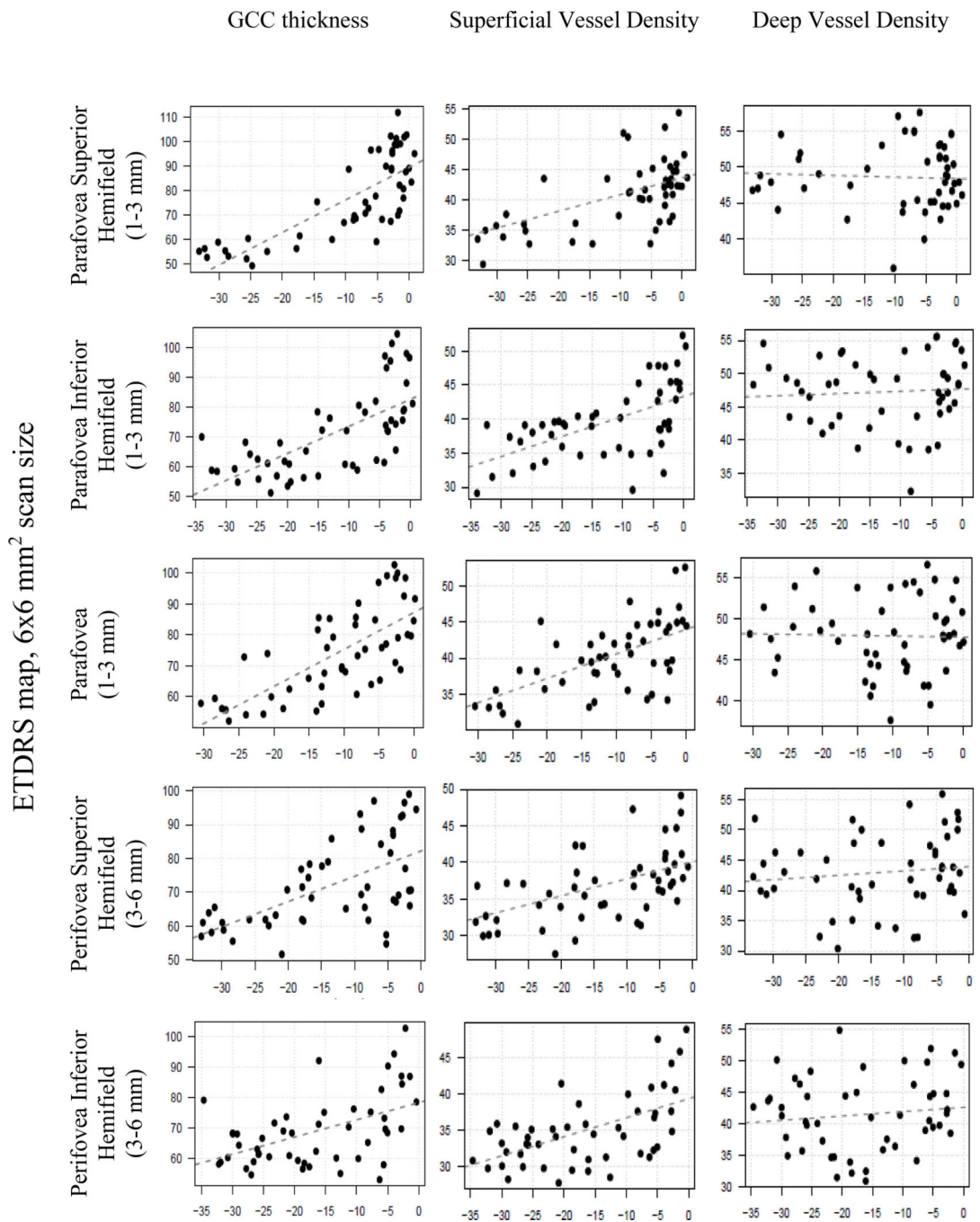
Figure 3.
Adjusted R^2 values with bootstrapped 95% confidence intervals for macular structure-function relationship in advanced glaucoma eyes using Optical Coherence Tomography Angiography (OCTA) superficial layer vessel density and Spectral Domain OCT Ganglion Cell Complex (GCC) thickness measurements with corresponding displaced visual field 10–2 mean sensitivity adjusted for retinal ganglion cell displacement. Consider Figures 1 and 2 for better correspondence of each region.
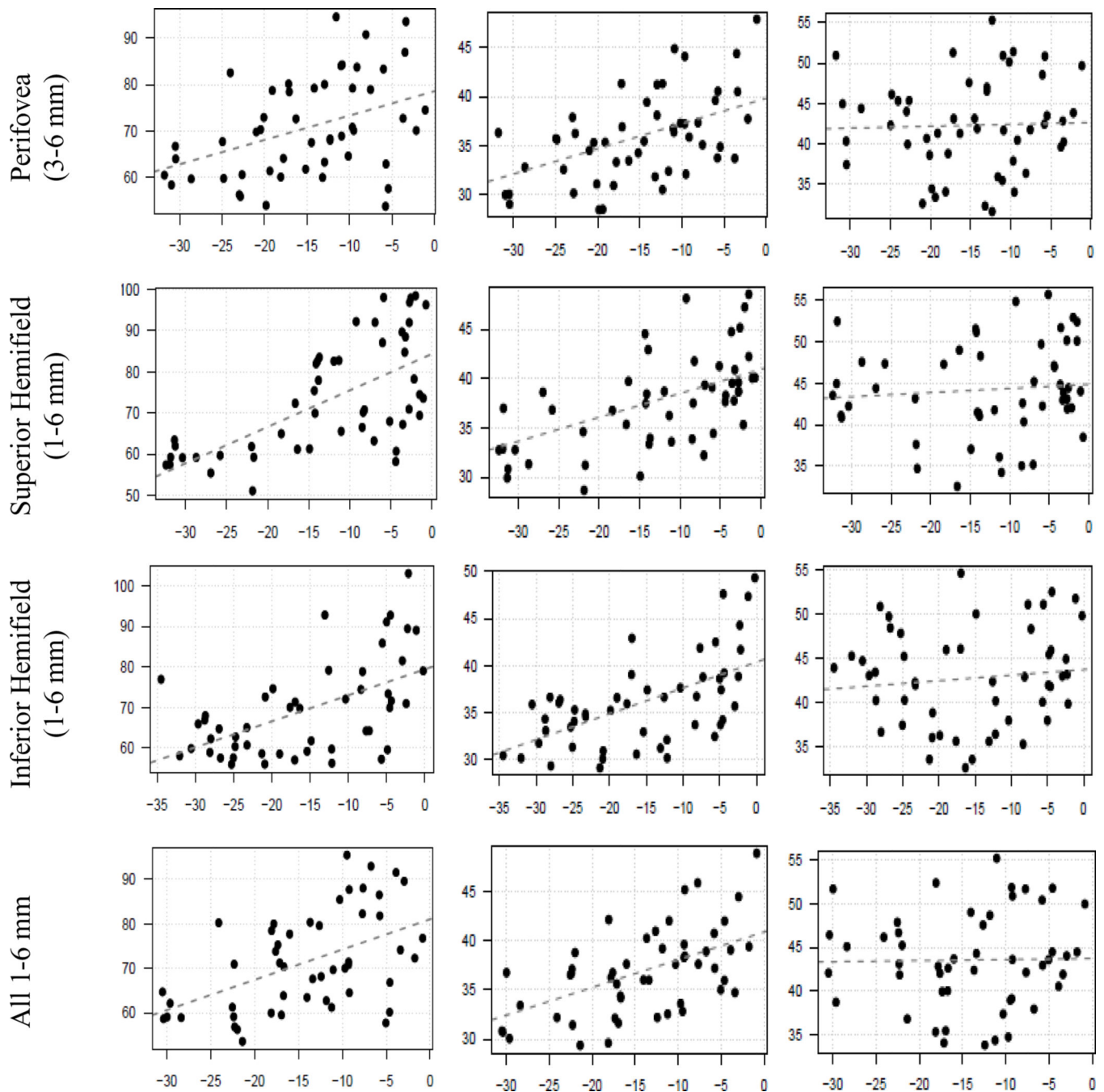
GCC thickness   Superficial Vessel Density   Deep Vessel Density

GCC thickness   Superficial Vessel Density   Deep Vessel Density

ETDRS map, 6x6 mm^2 scan size

Figure 4.
Scatter plots illustrating the best-fit linear regression line of regional and global macular structure-function association in advanced glaucoma eyes using Optical Coherence Tomography Angiography (OCTA) superficial and deep vessel density and Spectral Domain OCT Ganglion Cell Complex (GCC) thickness measurements (Y-axis) with corresponding displaced visual field 10–2 mean sensitivity adjusted for retinal ganglion cell displacement

(X-axis) by ETDRS map of 3×3 (Top) and 6×6 (Bottom) mm^2 scan sizes. Consider Figures 1 and 2 for better correspondence of each region.

Table 1:

Demographic and Ocular Characteristic of Study Population.

	N = 44 Patients (44 Eyes)
Age	72.4 (11.7) (44.2, 93.7) (65.6, 81.8)
Gender	
Female	16 (36.4%)
Male	28 (63.6%)
Race	
American Indian/ Alaska Native	1 (2.3%)
Asian	8 (18.2%)
Black or African American	5 (11.4%)
White	29 (65.9%)
Unknown or Not Reported	1 (2.3%)
Ethnicity	
Hispanic	1 (2.3%)
Not Hispanic	41 (93.2%)
Declined	2 (4.5%)
HTN	
No	22 (50.0%)
Yes	22 (50.0%)
Diabetes	
No	40 (90.9%)
Yes	4 (9.1%)
DBP (mmHg)	78.8 (11.4) (60.0, 110.0) (72.0, 84.0)
SBP (mmHg)	127.2 (18.3) (97.0,181.0) (118.0, 138.5)
VF 24–2 MD	−15.09 (4.86) (−30.10, −10.16) (−17.83, −11.48)
VF 24–2 PSD	10.95 (2.66) (5.20, 15.35) (9.35, 12.63)
VF 10–2 MD	−12.88 (7.23) (−30.30, −0.58) (−17.25, −8.08)
VF 10–2 PSD	9.69 (3.95) (1.35, 15.56) (7.43, 12.84)
IOP (mmHg) [*]	14.0 (6.72) (3.00,34.00) (9.25, 17.00)
Axial Length (mm)[+]	24.4 (1.93) (18.80, 30.07) (23.14, 25.10)
CCT (um)[+]	528.1 (37.11) (459.00, 593.00) (500.67, 560.33)
MOPP [*]**(mmHg)**	49.7 (9.28) (32.22, 73.11) (43.36, 56.06)

[*] 2 missing values +3 missing values.

HTN: hypertension; DBP: diastolic blood pressure; SBP: systolic blood pressure; VF 24–2 MD: visual field 24–2 mean deviation; VF 24–2 PSD: visual field 24–2 pattern standard deviation; IOP: intraocular pressure; CCT: central corneal thickness; MOPP: mean ocular perfusion pressure; Continuous variables are shown as mean (Standard Deviation) (Range) (First and Third Quartiles).

Table 6:

Summary of Multivariable Linear Models of Structure-Function Relationship of 3×3 mm and 6×6 mm Scan Sizes Optical Coherence Tomography Angiography (OCTA) Superficial Layer Vessel Density and Superficial Spectral Domain OCT Ganglion Cell Complex (GCC) Thickness Measurements with Corresponding Inferior Displaced Visual Field 10–2 Mean Sensitivity.

Scan Size		Superficial Vessel Density (%)		Superficial? GCC Thickness (μ)	
	ETDRS Map	*Estimate (95% CI)*	*p-value*	*Estimate (95% CI)*	*p-value*
3×3 mm	Para I Hemi (1–3mm)	0.40 (−0.29, 1.08)	0.250	0.34 (0.07, 0.61)	0.014*
	Para S Hemi (1–3mm)	0.31 (−0.17, 0.80)	0.194	0.31 (0.16, 0.47)	< 0.001***
	ParaFovea (1–3mm)	0.48 (−0.02, 0.98)	0.058	0.21 (0.03, 0.40)	0.026*
	Whole Image Grid Map				
	Whole Image I Hemi	0.43 (−0.28, 1.14)	0.224	0.36 (0.09, 0.64)	0.012*
	Whole Image S Hemi	0.26 (−0.28, 0.79)	0.334	0.34 (0.17, 0.52)	< 0.001***
	Whole Image	0.48 (−0.06, 1.01)	0.080	0.21 (0.02, 0.41)	0.036*
6×6mm	**ETDRS Map**				
	Para I Hemi (1–3mm)	0.84 (0.32, 1.37)	0.002**	0.31 (0.13, 0.50)	0.001**
	Para S Hemi (1–3mm)	0.46 (−0.03, 0.94)	0.064	0.36 (0.23, 0.49)	< 0.001***
	ParaFovea (1–3mm)	0.65 (0.21, 1.08)	0.004**	0.27 (0.14, 0.41)	< 0.001***
	Peri I Hemi (3–6mm)	0.87 (0.22, 1.52)	0.010**	0.19 (−0.07, 0.46)	0.149
	Peri S Hemi (3–6mm)	0.53 (−0.16, 1.22)	0.127	0.27 (0.05, 0.50)	0.020*
	PeriFovea (3–6mm)	0.63 (0.08, 1.19)	0.027*	0.10 (−0.11, 0.32)	0.335
	All I Hemi (1–6mm)	0.93 (0.30, 1.56)	0.005**	0.22 (−0.03, 0.46)	0.079
	All S Hemi (1–6mm)	0.54 (−0.12, 1.20)	0.108	0.31 (0.11, 0.51)	0.004**
	All (1–6mm)	0.67 (0.13, 1.21)	0.016*	0.16 (−0.04, 0.35)	0.113
	Whole Image Grid Map				
	Whole Image I Hemi	0.92 (0.27, 1.56)	0.007**	0.23 (−0.02, 0.49)	0.073
	Whole Image S Hemi	0.49 (−0.18, 1.17)	0.149	0.34 (0.12, 0.56)	0.003**
	Whole Image	0.62 (0.07, 1.18)	0.029*	0.17 (−0.05, 0.38)	0.122

*
Multivariable estimates are adjusted for GCC thickness, patient age, and the scan quality index.

S: Superior, I: Inferior. Hemi: Hemifield. Consider Figures 1 and 2 for better correspondence of each region.